Concomitant Studies of two F_{420} Cofactor Dependent Enzymes: Binding Isotherms of F_{420} Cofactor Dependent Glucose-6-phosphate Dehydrogenase and Kinetic Analysis of $F_{420}H_2$: $NADP^+$ Oxidoreductase Utilizing Isotope Effects Methods

by

SIQI DU

Presented to the Faculty of the Graduate School of

The University of Texas at Arlington in Partial Fulfillment

of the Requirements for the Degree of

MASTER OF SCIENCE IN CHEMISTRY

THE UNIVERSITY OF TEXAS AT ARLINGTON

August 2015

Acknowledgements

I would like to thank my advisor, Dr. Kayunta Johnson-Winters for her excellent mentorship and support during my graduate studies. She provided a working environment that allowed me to grow exponentially. Her guidance has aided me in acquiring problem solving capabilities and critical thinking skills.

In addition to Dr. Johnson-Winters, I would like to thank my committee members, Dr. Bradley Pierce and Dr. Subhrangsu Mandal, for their support and patience as I underwent the process of completing my thesis.

Also, I would like to thank all of my group members: Dr. Ebenezer Joseph, Mercy Oyugi, Toan Nguyen, Cuong Le, and Hasmat Ulah, for their endless support and encouragement. My work could not have progressed as rapidly as it did without their help in the lab. In addition, I would like to thank the Department of Chemistry and Biochemistry for providing me an opportunity to pursue my graduate studies.

Finally, I would like to thank my family and friends for their endless love. Without their support and encouragement, I would not have been able to complete my research or this degree.

August 11, 2015

Abstract

F_{420} cofactor, a flavin analogue, is a unique two electron carrier that has been found in a number of microorganisms. This thesis focuses on two F_{420}-dependent enzymes (F_{420}-dependent glucose-6-phosphate dehydrogenase and $F_{420}H_2$: $NADP^+$ Oxidoreductase). First, F_{420}-dependent glucose-6-phosphate dehydrogenase (FGD) from *Mycobacterium tuberculosis* has been shown to be essential for activation of the anti-TB prodrug PA-824. It has been suggested the Trp^{44} residue in the active side aids in the stabilization of possible intermediates during catalysis. Here, we examined the role of Trp^{44} during catalysis by creating the FGD W44A variant, which was catalytically inactive. However, we were able to isolate the W44A variant through gel filtration methods and then conduct binding studies. The results suggest that Trp^{44} aids in the binding of F_{420} cofactor to FGD, but not glucose-6-phosphate binding.

$F_{420}H_2$: $NADP^+$ Oxidoreductase (Fno) catalyzes the reversible reduction of $NADP^+$, producing NADPH via a hydride transfer from the reduced F_{420} cofactor. The focus of the Fno studies is to elucidate the reaction mechanism of Fno and to assess the probability of hydrogen tunneling within the enzyne. Kinetic isotope effect methods has been employed to examine the chemical steps of this enzymatic reaction. The results suggest that the hydride transfer in not the rate-limiting step. However, evidence shows the solvent plays an important role during this catalyzed reaction. Furthermore, no evidence of hydrogen tunneling is seen in this investigation.

Table of Contents

List of Illustrations

List of Tables

Chapter 1

Introduction

One of the distinguishing characteristics of methanogenic bacteria is their blue-yellow fluorescence when illuminated with UV light. This feature has been used as a means of identifying methanogenic bacteria in both wet mounts and solid growth media (1).This blue-yellow fluorescence arises from the presence of the F_{420} cofactor (Figure 1.1). F_{420} was first purified from *Methanobacterium* strain M.o.H by Cheeseman *et al*. (2) in 1972. Later, the structure of F_{420} was identified by Eirich *et al.* (3) in 1978 as N-(N-L-lactyl-γ-L-glutamyl)-L-glutamic acid phosphodiester of 7,8-didimethyl-8-hydroxy-5-deazariboflavin 5'-phosphate.

1.1 Structure of Cofactor F_{420}

The structure of cofactor F_{420} is shown in Figure1.1. The side chain attached at the N-10 position contains ribityl, phosphate, and lactyl groups in sequence. This is followed by several γ-glutamate groups. The number of γ-glutamate groups associated with F_{420} varies between one and nine depending upon the organism in which the cofactor is found (2, 3, 4, 5). It has been suggested that the type of glutamyl linkages, α- or β-linkage, can vary between species (2, 3, 4, 5).

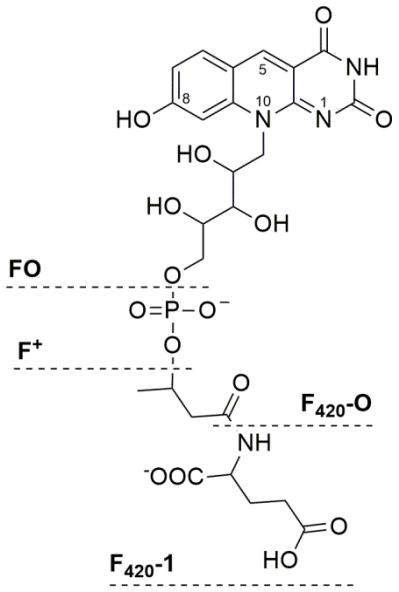

Figure 1.1 Structure of cofactor F_{420} and its precursors (2).

1.2 Spectral Properties and Chemistry of F_{420} Cofactor

F_{420} cofactor is spectrophotometrically distinct, having both oxidized and reduced forms (Figure 1.2). Reduction takes place via hydride transfer at the C5 of the 5'-deazaflavin of F_{420}, as shown in Figure 1.2. F_{420} is named for its intense absorbance at 420 nm. Upon reduction, F_{420} cofactor loses its absorbance at 420 nm, obtaining a new absorbance peak at 320 nm. F_{420} cofactor is pH-sensitive, displaying decreasing absorbance as pH decreases (1). As shown in Scheme 1.1, ionization of the 8-OH group (pK_a= 6.3) of F_{420} cofactor (Structure A) converts F_{420} cofactor into an anionic form, which has two resonance structures, B and C (6). This resonance hybrid is responsible for the long-wavelength absorbance of F_{420} cofactor at 420 nm. At basic pH values, deprotonation of the 3-N proton, pK_a= 12.2, produces structure D, resulting in the absorbance shift to a longer wavelength (6). The fluorescence of F_{420} is pH-dependent as

well. Ionization decreases the intensity of emission and also shifts both emission and excitation wavelengths (1). The reduced form of F_{420} has no fluorescence.

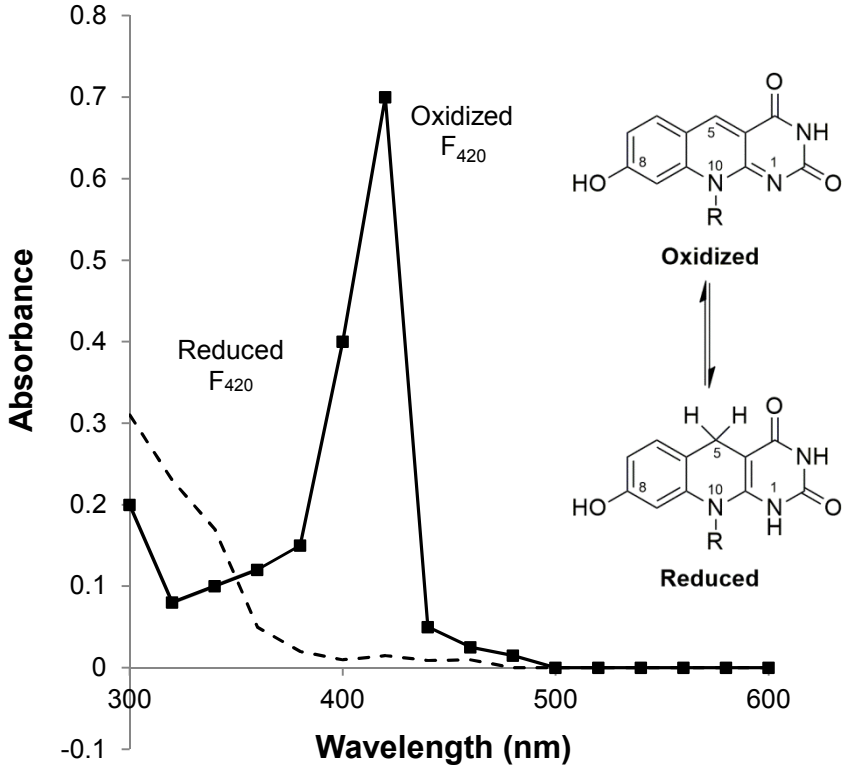

Figure 1.2 Visible spectra of reduced and oxidized F_{420} Cofactor (1).

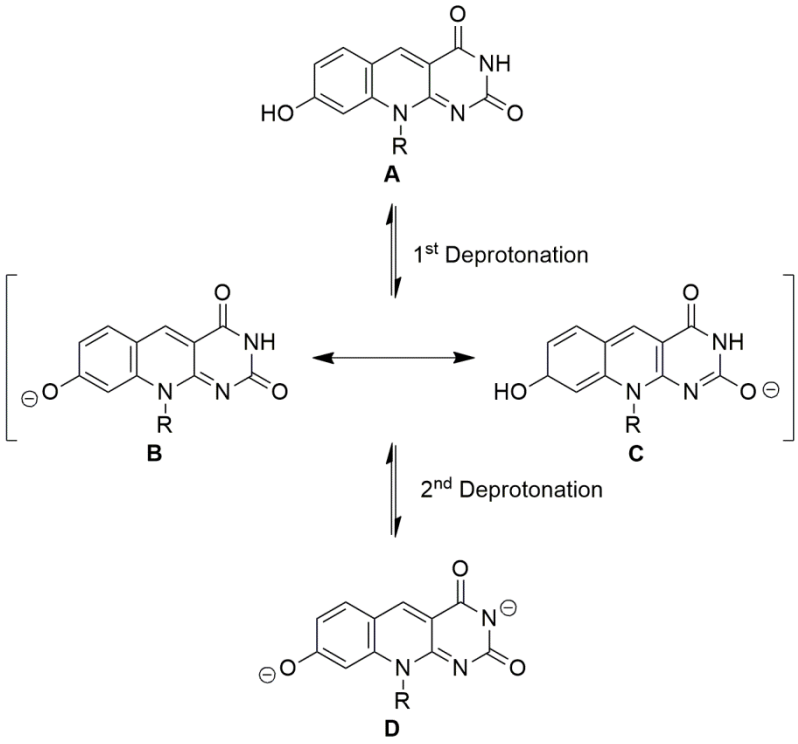

Scheme 1.1 Ionization and resonance structure of F_{420} Cofactor.

Examination of the structure shows F_{420} cofactor is a flavin analog, and would be expected to have analogous properties to structurally similar flavins, such as FMN and FAD (Figure 1.3) (7). However, it has been shown to be functionally similar to $NAD(P)^+$ (Figure 1.3). F_{420} is a two-electron carrier involved strictly in hydride transfer reactions. Its redox potential is -340 mV to -350 mV, which is more negative than the redox potential of $NAD(P)^+$ and FAD, as shown in Figure 1.4 (1).

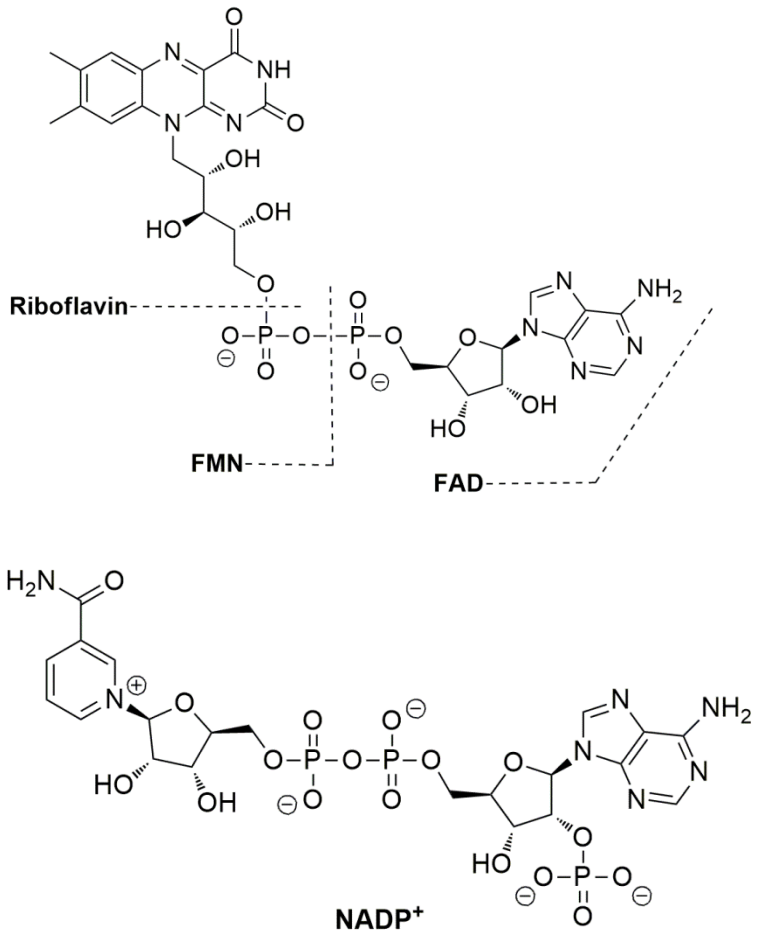

Figure 1.3 Structures of flavins and $NADP^+$ (7).

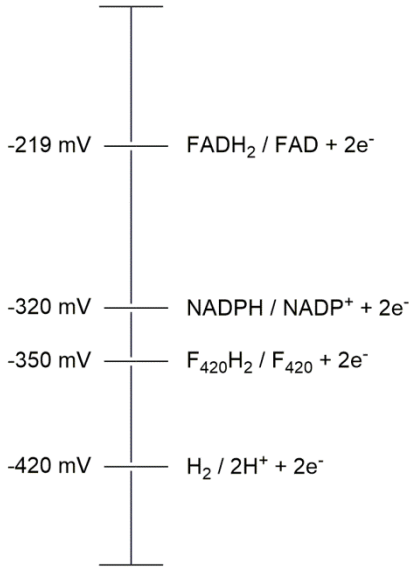

Figure 1.4 Reduction potential ladder (1)

1.3 Various F_{420}-Dependent Enzymes

Table 1 lists a number of F_{420} cofactor dependent enzymes. F_{420} was identified chemically in methanogenic archaea, where it functions as the coenzyme of oxidoreductases. In this strictly anaerobic microorganism, cofactor F_{420} is involved as a two-electron carrier in methane production (7, 8). F_{420} was later identified in non-methanogenic archaea, such as *Archaeoglobus fulgidus* (7, 9). F_{420} can be found in a number of other species such as, *Streptomyces*, where it is used in the biosynthesis of two antibiotics, lincomycin and tetracycline (4). This unique cofactor is also present in *Cyanobacteria* such as, *Synechococcus* and green alga *Scenedesmus* (10). F_{420} functions as the photosensitizer in DNA photolyases (9). However, F_{420} appears to be absent in most bacteria, plants and animals.

It has also been determined that all the F_{420}-dependent enzymes are *Si*-face stereospecific, with respect to C5 of the deazaflavin (11). This uniform stereospecificity of

all F_{420}-dependent enzymes is suprising, given that some flavin dependent proteins are *Si*-face stereospecific, while others are specific to *Re*-face (9).

Table 1.1 Deazaflavin-dependent reaction in different (micro) organisms.

Organism	Enzyme/Activity	Function	Refence
Archaea	F_{420} hydrogenase	Energy metabolism, Oxygen and sulfite detoxification, Oxygen sensing	12
	$F_{420}H_2$ dehydrogenase		13
	$F_{420}H_2$ oxidase		14
	$F_{420}H_2$: $NADP^+$ oxidoreductase		15
	$F_{420}H_2$: heterodisulfide oxidoreductase		16
	$F_{420}H_2$ quinone oxidoreductase		17
	F_{420}: formate dehydrogenase		18
	F_{420}: pyruvate synthase		19
	Methylenetetrahydromethanopterin dehydrogenase		20
	Methylenetetrahydromethanopterin reductase		21
	Secondary alcohol dehydrogenase		22
Actinobacteria	Deazaflavin-dependent nitroreductase	PA-824 activation	23
	Glucose-6-phosphate dehydrogenase	Providing $F_{420}H_2$	24
	$F_{420}H_2$-dependent reductases	Xenobiotic metabolism	25
Archaea, bacteria and eukaryotes	DNA photolyase	DNA repair and maintenance	26,27, 28,29

1.4 Synthesis and Purification of Cofactor F_{420}

F_{420} cofactor is not commercially available. Researchers who study F_{420}-dependent enzymes need to isolate it from microorganisms, or synthesize it using organic synthesis methods.

F_{420} has been previously purified from various microorganisms with different yields (7). In 2010, Ghader Bashiri *et al*. designed and prepared a new T7 promoter-based co-expression shuttle vector to co-express *Mtb* proteins in *M. smegmatis*. With the new vector, they achieved 10 times higher production levels of F_{420} compared with the wild type *M. smegmatis* strain (7).

Ashton *et al.* and Yoneda *et al.* reported the synthesis of FO (1976) and F_{420} (1979) respectively (Figure 1.5) (30, 31, 32). However, the intermediates in these synthetic preparations were extremely unstable. In 2015, Mohammad S. Hossain, Cuong Q. Le *et al.* developed a convenient synthesis of FO by improving the redox stability of synthetic intermediates, shown in Figure 1.6. This was achieved by utilizing a protection strategy that yielded stable intermediates, improved yields, and simplified purification by allowing the use of flash chromatography (30).

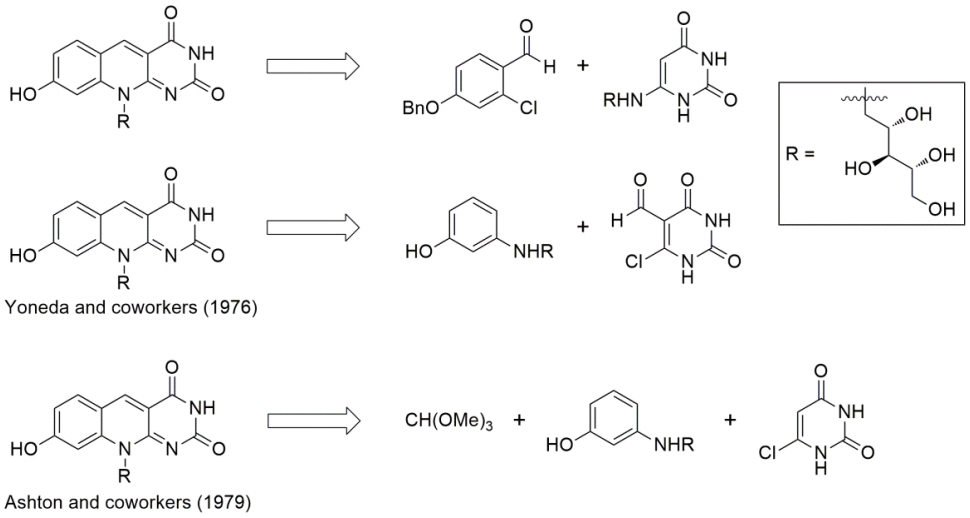

Figure 1.5 Prior syntheses of compounds FO and F_{420} (30, 31, 32).

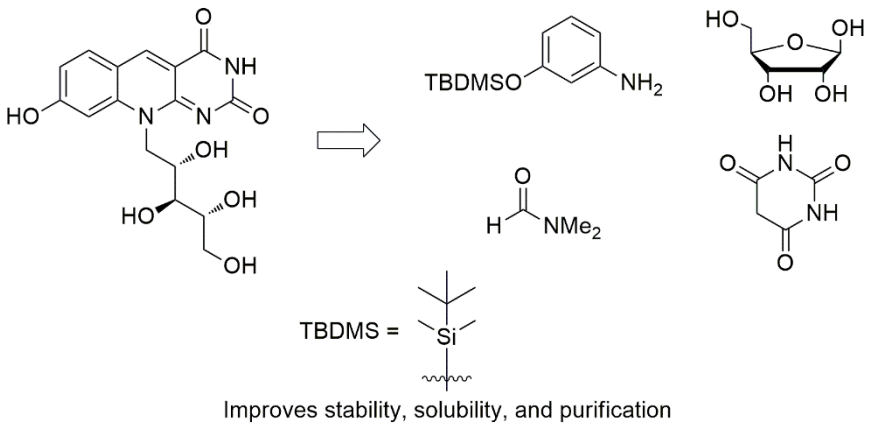

Figure 1.6 Retrosynthesis of FO utilizing protected 3-aminophenol (30).

Chapter 2

F_{420} cofactor dependent glucose-6-phosphate dehydrogenase (FGD)

2.1 Introduction

2.1.1 Tuberculosis

Tuberculosis (TB) is currently the second highest cause of death from an infectious disease and the biggest killer of people who are infected with HIV (33). It is estimated that *Mycobacterium tuberculosis (Mtb) bacilli*, the causative agent of TB, infects one-third of the world's population (34). TB is usually a chronic and slowly progressing disease. Current TB chemotherapy consists of a six-month-long regiment with at least four drugs (35, 36, 37). A growing problem is the emergence of *Mtb* strains resistant to the drugs used in the treatment progress.

2.1.2 New Anti-TB Pharmaceuticals

However, only a few novel anti-TB pharmaceuticals have been developed over the last several decades. PA-824, a nitroimidazopyran compound (Figure 2.1) with potent bactericidal activity against both replicating and non-replicating *Mtb*, is a promising anti-TB drug that is currently undergoing a clinical trial with the Global Alliance for TB Drug Development (4). PA-824 is a pro-drug whose activation involves an enzyme found in *Mtb*, F_{420} cofactor dependent glucose-6-phosphate dehydrogenase (FGD). Recent studies have shown that FGD does not directly activate PA-824, but it provides the electrons from the reduced F_{420} cofactor to an accessory protein, deazaflavin dependent nitroreductase (Ddn), which in turn activates PA-824 (4).

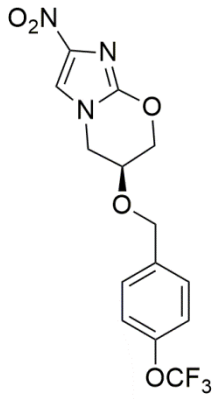

Figure 2.1 Chemical structure of PA-824 (35).

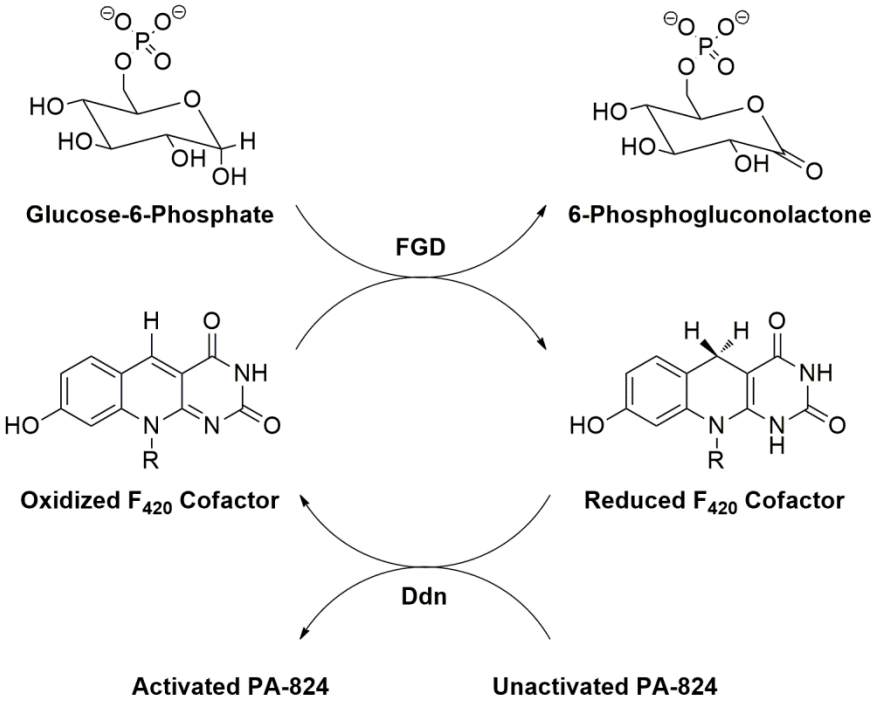

Scheme 2.1 Role of FGD in the F_{420}-dependent reductive activation of PA-824 (4).

2.1.3 F_{420} Cofactor Dependent Glucose-6-phosphate Dehydrogenase (FGD)

FGD, found only in *Mycobacteria* and *Nocardia* species, is an unusual glucose-6-phosphate dehydrogenase that uses F_{420} instead of NADP as a cofactor to catalyze the

conversion of glucose-6-phosphate to 6-phosphogluconolactone (Scheme 2.1). FGD uses glucose-6-phosphate to transfer hydride to the oxidized form of the F_{420}, thus yielding the reduced form of the cofactor, $F_{420}H_2$ and oxidized product (6-phosphogluconolactone). In 2008, Ghader Bashiri and co-workers determined the crystal structure of FGD with and without bound F_{420} (Figure 2.2) (4). FGD is a 78 kDa homodimer. Each monomer of FGD forms $(\alpha/\beta)_8$ TIM-barrel motif. The proposed FGD catalytic mechanism (Scheme 2.2) suggests that His^{40} acts as a catalytic base, initiating the reaction by deprotonating the O1 hydroxyl group of glucose-6-phosphate (G6P). The reaction then continues with the hydride transfer from C1 of G6P to C5 of F_{420}. The negatively charged reaction intermediate would be stabilized by the hydrogen bonds from Trp^{44} and Glu^{13} (4).

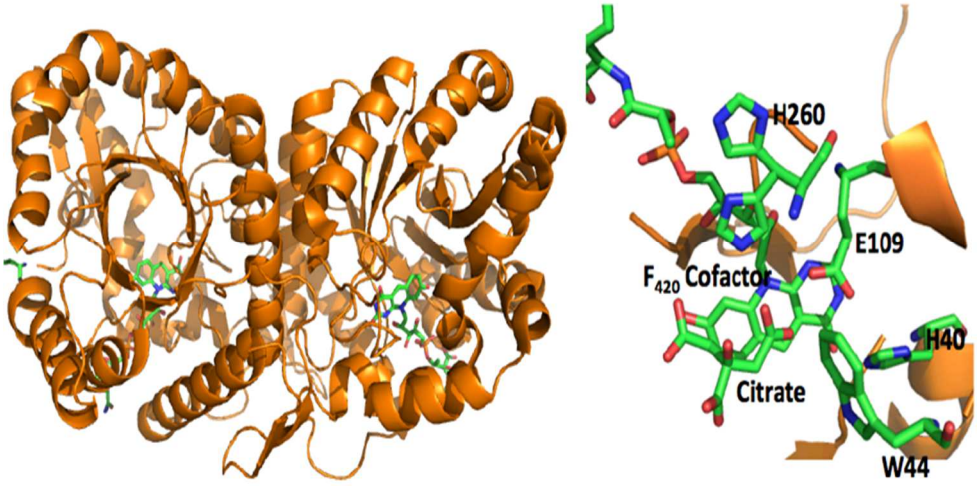

Figure 2.2 Crystal structure of *M. tuberculosis* FGD, PDB ID–3C8N, resolution 1.90 Å (4).

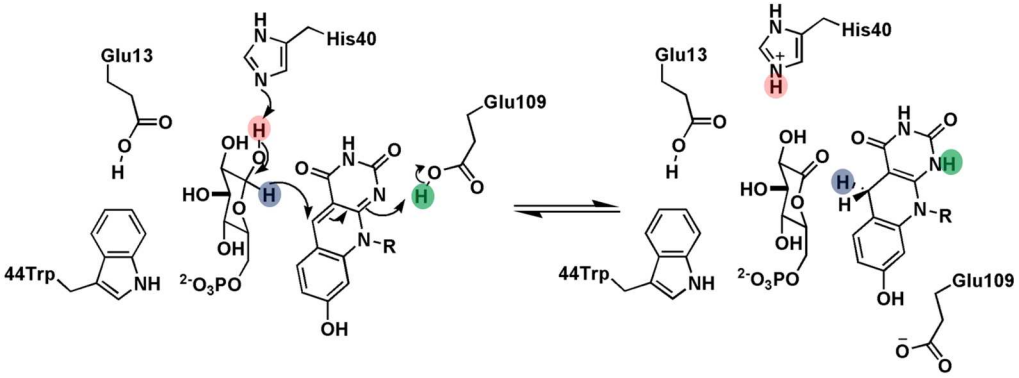

Scheme 2.2 Proposed catalytic mechanism of FGD (4).

2.1.4 Motivation of FGD Studies

It was suggested that Trp^{44} would help to stabilize the intermediate during the enzymatic reaction. However, there has not sufficient studies on this amino acid residue to fully support this hypothesis. In order to determine the role of Trp^{44} during the reaction, the FGD W44A variant was created and studied.

2.2 Material and Methods

2.2.1 Reagents

Cofactor F_{420} was provided by Dr.Edward N. Baker from Maurice Wilkins Center for Molecular Biodiscovery and Laboratory of Structural Biology. LB Broth was purchased from US Biologicals. Tween 80 was purchased from Acros Organics. BME (β-mercaptoethanol), imidazole, kanamycin, hygromycin, glycerol, and Tris buffer were purchased from Fisher Scientific.

2.2.2 Electroporation of M. Smegmatis

pYUB FGD W44A construct was transformed into the *M. smegmatis* strain mc^24517 (both kindly provided by Dr. Edward N. Baker, Maurice Wilkins Center for Molecular Biodiscovery and Laboratory of Structural Biology) for expression. A volume of 40 μL of *M. smegmatis* mc^24517 cells were mixed with 1 μL of expression construct and

260 μL of 10% glycerol in a 0.2 cm electrode gap cuvette. A Bio-Rad Gene Pulser (set at R = 1000 Ω, Q = 25 μF and V = 2.5 kV) was used to perform electroporation (kindly provided by Professor Shawn Christensen, the University of Texas at Arlington). Cells were harvested with 1 ml of 7H9/ADC/Tween (containing Middlebrook 7H9 (Difco)), 10% ADC (albumin/dextrose/catalase) and 0.05% Tween 80) and incubated for 3 hours at 37 °C with shaking, and then plated on 7H10/ADC/Tween plates containing 50 μg/ml each of kanamycin and hygromycin B, and incubated for 2 ~ 3 days at 37 °C (38, 39).

2.2.3 Expression of FGD W44A

Single transformed colonies were selected from the plates and incubated in LB medium supplemented with 0.05% Tween 80 and 50 μg/ml each of kanamycin and hygromycin B at 37 °C for 2 days. Autoinduction medium ZYM-5052 was used for FGD W44A expression (1% N-Z-amine AS, 0.5% yeast extract, 25 mM Na_2HPO_4, 25 mM KH_2PO_4, 50 mM NH_4Cl, 5 mM Na_2SO_4, 2 mM $MgSO_4$, 1x trace metals, 0.5% Tween 80). Expression cultures were grown in a shaking incubator for 4 days at 37 °C (38, 39).

2.2.4 Purification of FGD W44A

2.2.4.1 Sonication

Cells from *M. smegmatis* expression cultures were harvested by centrifuging at 6000 rpm for 30 minutes at 4 °C. Cell pellets were resuspended in a lysis buffer (50 mM Tris-HCl/150 mM NaCl/1 mM BME/10 mM imidazole, pH 7.0) in the presence of protease inhibitor (38, 39). The cells were then lysed by sonicating for 5 seconds, with 59.9 seconds resting interval, for a total of 4 minutes.

2.2.4.2 Ni-affinity Chromatography

The soluble fraction containing His-tagged FGD W44A was separated from the insoluble material by centrifuge at 5000 rpm for 60 minutes. The supernatant was then loaded onto a Ni-NTA column from Sigma, (2.5 x 6 cm), which was previously

equilibrated with afore-mentioned lysis buffer. The column was then washed with washing buffer (50 mM Tris-HCl/150 mM NaCl/1 mM BME/25 mM imidazole, pH 7.0) and eluted with an imidazole gradient of 25-500 mM (38, 39). The active fractions containing FGD1 W44A were combined and concentrated by filtration (Millipore, 30 kDa cut-off) to about 1 mL.

2.2.4.3 Size Exclusion Chromatography

The 1 mL sample was loaded onto a 1 x 40 cm size exclusion column (Sephacryl S-200 HR from GE Healthcare). The column was previously equilibrated with 50 mM Tris-HCl/300 mM NaCl buffer, pH 7.0. All chromatography steps were operated at 4 °C using a Bio-Rad FPLC system (38, 39).

2.2.5 SDS-PAGE

Sub-samples of each purification step were used for the SDS-PAGE analysis. To prepare the sample, 6 μl of each FGD W44A sub-samples were mixed with 6 μL of loading dye. The samples were heated in boiling water for 10 minutes. The protein marker was loaded into the first lane. Then the prepared samples were loaded into subsequent wells. Electrophoresis was run for 50 minutes at 150 V. The gel was washed with DI water for 10 minutes, then stained using Coomassie blue (G-250).

2.2.6 Quantification of Protein

The concentration of the pure protein was determined using Bradford reagent at 595 nm. 1.5 mL of Bradford reagent and 30 μL of 50 mM Tris-HCl/300 mM NaCl (pH 7.0) buffer were used as a blank at 595 nm. Then the absorbance of 1.5 mL of Bradford reagent and 30 μL of diluted protein sample was measured at 595 nm. Based on a protein standard curve, using bovine serum albumin as the standard, the concentration of FGD W44A was calculated.

2.2.7 Storage of Protein

The purified protein was stored at -80 °C in 50 mM Tris-HCl/300 mM NaCl (pH 7.0) buffer in the presence of 20% glycerol.

2.2.8 Binding Assay of F_{420} and Glucose-6-Phosphate

Binding studies were performed using fluorescence spectroscopy (Horiba FluoroMax Spectrofluorometer). The binding assays were monitored in a Spectrosil® Quartz sub-micro cell (160 µl nominal volume) from Starna Cells. The excitation and emission slit widths were 8 nm. The samples were excited at 290 nm and the emission scan was performed between 310-500 nm.

To obtain the dissociation constant (K_d) of F_{420}, 0.35 µM of FGD W44A was titrated with varying concentrations of F_{420} (0-3 µM) in 50 mM Tris-HCl (pH 7.0) buffer.

To obtain the K_d of G6P, 0.35 µM of FGD W44A was titrated with varying concentrations of G6P (0-0.75 mM) in 50 mM Tris-HCl (pH 7.0) buffer.

The extent of substrate binding to FGD W44A was determined by monitoring changes in maximal fluorescence emission at 340 nm (44). The K_d value was calculated by fitting the relative change in intrinsic fluorescence at 340 nm of FGD W44A vs. substrate concentration to a one-site binding (hyperbolic model) using non-linear regression.

$$\mathrm{F}_{340} = \frac{F_{max}[S]}{K_d+[S]} \qquad \text{Equation 1}$$

2.3 Results

2.3.1 FGD Binding Experiments

A decrease in fluorescence intensity at 340 nm was observed for both F_{420} and glucose-6-phosphate titration, as the concentration of substrate bound to FGD W44A increased. Upon addition of F_{420} or G6P, the tryptophan fluorescence of FGD W44A is

quenched indicating a change in the tryptophan environment (17). The strong change in fluorescence intensity provides an excellent method of measuring the dissociation constants (K_d) of F_{420} and G6P (Figure 2.3, table 2.1). From these fluorescence data, K_d for F_{420} binding was determined to be 18.1 ± 2.2 nM. The binding data for G6P gave a K_d of 16.1 ± 0.6 µM.

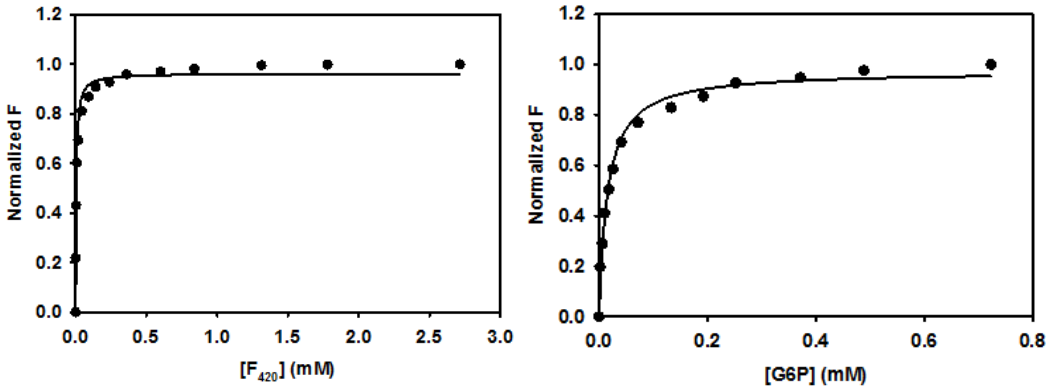

(a) (b)

Figure 2.3 Binding of (a) F_{420} to FGD W44A,(b) G6P to FGD W44A

For *wt*FGD, the K_d for F_{420} binding was 8.7 ± 0.7 nM, and K_d of G6P 16.7 ± 4.0 µM, as shown in Figure 2.4 (performed by Mercy Oyugi).

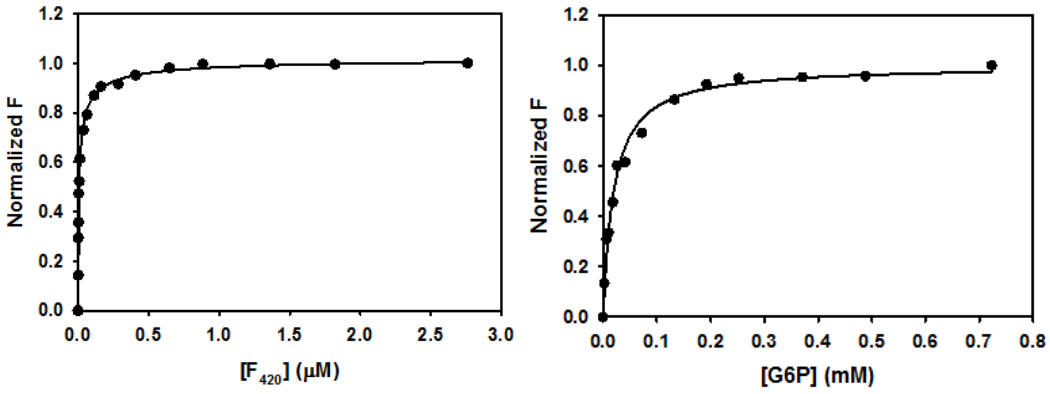

(a) (b)

Figure 2.4 Binding of (a) F_{420} to wtFGD, (b) G6P to *wt*FGD

2.4 Discussion

As shown in Table 2.1, the G6P K_d values for both *wt*FGD and FGD W44A were approximately the same, 16 μM. However, the K_d of F_{420} for FGD W44A is about two-fold larger than that for *wt*FGD, which means that FGD W44A has lost some affinity for the F_{420} cofactor in comparison to *wt*FGD. We are able to conclude here, that W44 aids in cofactor binding, but not G6P binding. According to the crystal structure, the distance between citrate, the competitive inhibitor, and Trp^{44} is 3 Å, while the distance between F_{420} cofactor and Trp^{44} is 6 Å. Our results indicate that the crystal structure may not be true structure. Enzyme could experience conformational change in solution. Or the citrate location in crystal structure may not be the actual location where G6P would bind to.

Since FGD W44A showed no catalytic activity, one can conclude that the W44 residue plays a significant role in the active site, and the enzyme will not tolerate a significant change at that position. With this in mind, further studies involving new mutants which use residues that still allow for hydrogen bonding, but vary the hydrogen's distance to the substrate in the active site, should be investigated. A W44H mutant would

be the closest to the original tryptophan residue in distance and would retain aromatic properties, while eliminating the additional four carbons, leaving a single imidazole ring instead of the bicyclic indole motif. Also, W44F would place the hydrogen further out into the active site, while a W44S mutant would decrease the distance. Experiments involving these mutants should provide a better understanding as to the function of theTrp^{44} residue.

Table 2.1 Binding Assay Parameters

	K_d of F_{420}	K_d of G6P
wtFGD	8.7 ± 0.7 nM	17 ± 4 μM
FDG W44A	18 ± 2 nM	16.1 ± 0.6 μM

Chapter 3

wt$F_{420}H_2$:$NADP^+$ oxidoreductase (Fno)

3.1 Introduction

3.1.1 F_{420}: $NADP^+$ Oxidoreductase (Fno)

F_{420}-dependent $NADP^+$ oxidoreductase (Fno) is an enzyme that catalyzes the reversible reduction of $NADP^+$ to NADPH. The reduced F_{420} cofactor transfers the hydride to oxidized $NADP^+$, producing NADPH (Scheme 3.1). This hydride transfer occurs stereospecifically from the *Si-face* of the F_{420} cofactor (C5 position) toward the *Si-face* of $NADP^+$ (C4 position) (40).

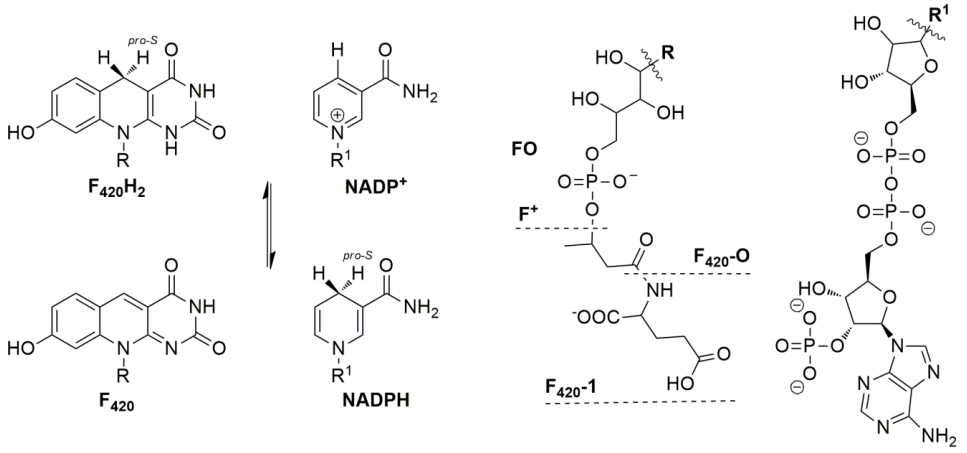

Scheme 3.1 Fno catalyzes the reversible reduction of NADPH (40).

Fno is found in methanogenic, halophilic, and sulfate-reducing archaea (8), and has been purified from *Archaeoglobus fulgidus* (9),*Methanobaterium thermoautotrophicum* (41), *Methanococcus vannielii* (40), *Methanogenium organophilum* (6), *Halobacterium cutirubrum* (42) and *Streptomyces griseus* (43). In some organisms, such as *Archaeoglobus fulgidus*, Fno has been shown to be homodimeric, while in

others, such as *Methanobacterium thermoautotrophicum*, it is a homotetrameric enzyme (6, 9).

The crystal structure of Fno from *A. fulgidus*, Figure 3.1, was solved in 2001 (9). This homodimeric enzyme has an α,β twisted fold. The distance between C5 of F_{420} and C4 of NADP is 3.1 Å, which is optimal for hydride transfer (9).

Previous research performed in our by Dr. Ebenezer Joseph and Cuong Quang Le *et al.* suggested that Fno is a regulatory enzyme with half-site activity and negative cooperativity (44). Based upon the pre-steady state kinetic data, only 50% of FO was reduced in the first burst phase, supporting the half-site reactivity of Fno. A double reciprocal plot with NADPH showed a downward curvature at high concentration of NADPH, suggesting negative cooperativity. This negative cooperativity is explained in detail by the Koshland-Nemethy-Filmer (KNF) model (45). They proposed that FO and NADPH initially bound to the active site of one monomer. The binding of the substrates to the first monomer induced conformational change of the second monomer, resulting in a lower affinity for substrates. After the first hydride transfer, the products were released form the active site upon binding of FO and NADPH into the active site of the second monomer. These steps were followed by a second hydride transfer and products were released from the second monomer (44)

3.1.2 Kinetic Isotope Effect

A major problem in studying the kinetic mechanism of a given enzyme is that enzymatic transformations take place via multiple steps. Measurements of steady state and even pre-steady state kinetics do not indicate which microscopic steps are being studied (46). Most enzyme reactions consist of a series of events, such as binding of substrates, conformational changes of enzyme, and release of products, each of which can affect the experimental measurements. Kinetic isotope effect is one of the most

powerful tools available to isolate the bond-cleavage steps from nonisotopic binding/cleavage steps and protein conformational changes (46).

A Kinetic isotope effect (KIE) is defined as the ratio of rate constants for the reactions involving the light (k_L) and the heavy (k_H) isotopically substituted reactants:

$$\text{KIE} = \frac{k_L}{k_H}$$

Two types of KIEs can be defined: primary KIE and secondary KIE. Primary (1°) KIE is observed when the bond being formed or broken is connected to the isotopically labeled atom, and the bond forming/breaking occurs in the rate-limiting step. Secondary (2°) KIE is observed where the labeled atom does not participate in the bond formation or cleavage, but is typically one or two bonds away. The hydrogen KIE is particularly useful because the mass ratio of its isotopes is larger than that of any other element, resulting in relatively large KIEs (47).

3.1.3 Hydrogen Tunneling

In an enzymatic reaction, as the reacting bond climbs the energy barrier, it reaches a position where the wavelength of its particle exceeds the barrier width (46, 48). At this point, products can be formed without having to overcome the energy barrier of the transition state (46). This quantum effect is denoted as tunneling, because the particle seems to "dig" a tunnel through the barrier (46).

Numerous experimental and theoretical data suggest that tunneling occurs in a large number of enzyme catalyzed hydrogen/hydride transfer reactions (48, 49 50, 51). Owing to the quantum-mechanical nature of a hydrogen transfer reaction, the rate of the transfer is sensitive to the protein's motions that modulate the height and the width of the reaction's barrier (48, 51).

Dihydrofolate reductase (DHFR), catalyzes the reduction of 7,8-dihydrofolate (H_2folate) to 5,6,7,8-tetrahydrofolate (H_4folate), has been examined as a model for hydride transfer study (48, 51). In that study, Ile14 has been replaced with alanine by site-directed mutagenesis and kinetic isotope effect method was employed. The data showed the hydride transfer rate was 450 s^{-1} for *wt*DHFR, whereas for I14A DHFR the rate was decreased ~ 14 fold, suggesting that reorganization to the tunneling-ready conformation is altered by the alanine mutation in such way that H-tunneling is less efficient (48, 51).

3.1.4 Motivation of Fno Studies

Fno is an enzyme that catalyzes the reversible reduction of $NADP^+$ to NADPH within archaea and is essential for controlling NADPH concentrations and related cellular function. However, there exists no thorough understanding of Fno's kinetics or mechanism. Here, we would like to investigate the reaction mechanism of Fno and to assess the probability of hydrogen tunneling within the enzyme utilizing the kinetic isotope effect methods. This technique was used to probe the hydride transfer and to aid in determining the rate-limiting step during Fno catalysis.

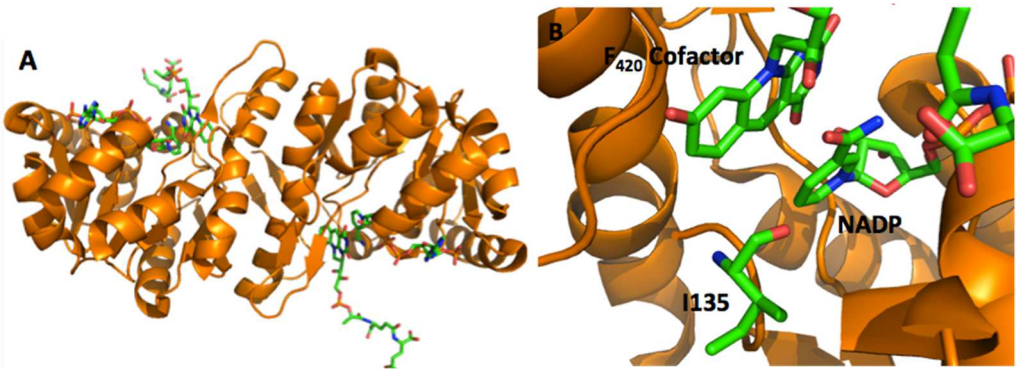

Figure 3.1 Crystal structure of Fno. A: homodimeric overall fold of Fno, in the presence of the F_{420} cofactor and NADP. B: active site of Fno, PDB ID-1JAX, resolurion1.65Å (9).

3.2 Material and Methods

3.2.1 Reagents

FO was synthesized by Mohammad Hossain in the laboratory of Dr. Frank Foss (The University of Texas at Arlington, Department of Chemistry and Biochemistry). NADPD and NADPH were synthesized in the laboratory of Dr. Pablo Sobrado (Virginia Tech, Department of Biochemistry). The pET24b plasmid used for Fno gene insertion was purchased from Novagen. LB Broth was purchased from US Biologicals. Isopropyl β-D-1-thiogalactopyranoside (IPTG) was purchased from Gold Biotechnology. Potassium phosphate dibasic buffer was purchased from Amresco. MES buffer was purchased from Acros Organics. *E. coli* C41*DE3* cells were purchased from Lucigen. Kanamycin, Tris buffer and ammonium sulfate were purchased from Fisher Scientific.

3.2.2 Expression

The Fno gene from *A. fulgidus* was cloned into pET24b vector. The plasmid was then transformed into C41(DE3) *E. coli* according to Agilent Technologies protocol.

The frozen *E. coli* C41(DE3) cell stock containing the Fno gene in pET24b plasmid was inoculated in a 10 L LB culture at 37 °C in the presence of 50 μg/ml kanamycin. The culture then was induced with 1 mM IPTG at an OD_{600} of 0.6.

3.2.3 Purification of Fno

3.2.3.1 Sonication

Cells were harvested by centrifuging at 6000 rpm for 30 minutes at 4 °C. The cell pellet was re-suspended in 1.5 M potassium phosphate buffer, pH 8.0 for 20 minutes. The cells were then lysed by sonicating for 1.5 minutes, with 30 seconds resting interval, for a total of 6 minutes.

3.2.3.2 Heat Precipitation

After centrifugation at 8000 rpm for 30 minutes, the supernatant was heated in a water bath at 90 °C for 30 minutes and cooled down to room temperature, then centrifuged again at 8000 rpm for 30 minutes.

3.2.3.3 Ammonium Sulfate Fractionation

Ammonium sulfate (40%) was added into the supernatant and centrifuged at 8000 rpm for 30 minutes. The resulting supernatant was saved, and the pellet was discarded. The 40% $(NH_4)_2SO_4$ supernatant was saturated to 70% $(NH_4)_2SO_4$ and centrifuged at 8000 rpm for 30 minutes. The resulting supernatant was discarded, while the 40-70% $(NH_4)_2SO_4$ pellet was saved for further purification.

3.2.3.4 PEI Precipitation

The 40-70% $(NH_4)_2SO_4$ pellet was re-suspended in 50 mM Tris-HCl buffer, pH 7.5, and was treated with 0.05% polyethylenimine (PEI) to precipitate nucleic acids.

3.2.3.5 Dialysis

After centrifuging at 8000 rpm for 10 minutes, the resulting supernatant was dialyzed in 2 L of 50 mM Tris-HCl/50 mM NaCl buffer, pH 7.5 at 4 °C overnight. The dialysis solution was centrifuged for 20 minutes, and the pellet was discarded. The supernatant was kept for chromatography analysis.

3.2.3.6 Anion Exchange Chromatography

The resulting dialysis supernatant was loaded onto a DEAE-cellulose column from Sigma, 2.5 x 6 cm, which was equilibrated with 50 mM Tris-HCl/100 mM NaCl (pH 7.5). The column was then washed with 50 mM Tris-HCl/100 mM NaCl (pH 7.5) and eluted with 50 mM Tris-HCl/250 mM NaCl (pH 7.5). The active *wt*Fno fractions were combined and concentrated by filtration (Millipore, 30 kDa cut-off) to 1 mL.

3.2.3.7 Size Exclusion Chromatography

The 1 mL sample was loaded onto a 1 x 40 cm size exclusion column (Sephacryl S-200 HR from GE Healthcare). The column was previously equilibrated with two column volumes of 50 mM MES/NaOH (pH 6.5). All the column chromatography steps were carried at 4 ˚C and a flow rate of 1 mL/min using a Bio-Rad FPLC system.

3.2.4 SDS-PAGE

Sub-samples of each purification step were used for the SDS-PAGE analysis. To prepare the sample, 6 µl of each Fno sub-samples was mixed with 6 µL of loading dye. The samples were heated in boiling water for 10 minutes. The protein marker was loaded into the first lane. Then the prepared samples were loaded into subsequent wells. Electrophoresis was run for 50 minutes at 150 V. The gel was washed with DI water for 10 minutes, then stained using Coomassie blue (G-250).

3.2.5 Quantification of Protein

The concentration of the pure protein was determined using Bradford reagent at 595 nm.1.5 mL of Bradford reagent and 30 µL of 50 mM MES/NaOH (pH 6.5) buffer were used as a blank at 595 nm. Then the absorbance of 1.5 mL of Bradford reagent and 30 µL of diluted protein sample at 595 nm. Based on a protein standard curve, using bovine serum albumin as the standard, the concentration of *wt*Fno was calculated.

3.2.6 Storage of Protein

The purified protein was stored at -80 °C in 50 mM MES/NaOH (pH 6.5) buffer in the presence of 20% glycerol.

3.2.7 Steady State Kinetics of wtFno

All the steady-state kinetic measurements were carried out in a Spectrosil® Quartz sub-micro cell (160 µl nominal volume) from Starna Cells using a Cary 100 UV-Visible spectrophotometer.

The concentrations of NADPH and FO were determined by Beer's Law

$$A = \varepsilon\, l\, c$$

Where A is the absorbance, ε is the extinction coefficient, l is the cell path length, and c is the analyte concentration. The extinction coefficient of NADPH and FO are 6.22 $mM^{-1}cm^{-1}$ at 340 nm (in 50mM Tris-HCl buffer, pH 7.4) and 41.4 $mM^{-1}cm^{-1}$ at 420 nm (in 50mM Potassium Phosphate buffer, pH 7.0) respectively (52).The extinction coefficient for FO is assumed to be the same as F_{420} cofactor.

3.2.7.1 Solvent Kinetic Isotope Effect

3.2.7.1.1 Steady state kinetics of *wt*Fno in H_2O

The reaction mixture contained FO and NADPH in 50 mM MES/NaOH buffer, pH 6.5, at 22 °C. The reaction was initiated by adding Fno to a final concentration of 22 nM in a final volume of 200 µL. Reaction progress was monitored by following FO reduction at 420 nm.

To determine apparent FO kinetic parameters, FO concentrations were varied from 3 µM to 30 µM, while NADPH concentration was held constant at 600 µM. For determining apparent NADPH kinetic parameters, FO concentration was held constant at 25 µM, while NADPH concentrations varied from 3 µM to 1000 µM.

The initial rate of the reaction was calculated using an extinction coefficient of 34.7 $mM^{-1}cm^{-1}$ for FO at pH 6.5 at 420 nm. The initial rate was converted to the macroscopic rate constant by dividing by the concentration of enzyme. A plot of rate constant vs substrate concentration was used to determine the steady-state kinetic parameters (Equation 2).

$$k = \frac{k_{cat}\,[S]}{K_m + [S]} \qquad \text{Equation 2}$$

The kinetic data for NADPH were plotted using the double reciprocal plot equation,

$$1/k = (K_m/k_{cat})(1/[S] + (1/k_{cat}) \quad \text{Equation 3}$$

where, k is the first order macroscopic rate constant, or turnover number, obtained by dividing the initial rate by the enzyme concentration; K_m is the Michaelis-Menten constant and [S] is concentration of NADPH. The individual rate constants and K_m for the two phases were obtained from linear fits of the two phases.

3.2.7.1.2 Steady state kinetics of *wt*Fno in D_2O

The experiments were performed under similar conditions as described in 3.2.7.1.1 Solvent KIE (in H_2O), except the buffer used was a 50 mM MES/NaOD, pH 6.1, using D_2O instead of H_2O as the solvent.

3.2.7.2 Substrate Kinetic Isotope Effect

The experiments were performed under similar conditions as described in 3.2.7.1.1 Solvent KIE in H_2O, except the substrates used were the NADPH and NADPD synthesized in the laboratory of Dr. Pablo Sobrado, not commercial products.

3.2.8 Single Turnover Kinetics

3.2.8.1 Solvent Kinetic Isotope Effect

The single turnover experiments were performed in the Hitech Scientific DX2 stopped-flow spectrophotometer at 22 °C. Time trace measurements were made in diode-array mode between 350-800 nm following FO reduction at 420 nm.

*wt*Fno (20 μM), FO (4 μM) and NADPH (600 μM) were used for single-turnover kinetic studies. The solvents used were H_2O and D_2O respectively. The data was fit into the double parameter exponential decay equation:

$$\text{Absorbance} = a*e^{(-k*t)} + c*e^{(-d*t)} + y_0 \qquad \text{Equation 4}$$

Where, a is the amplitude for fast phase, *k* is the rate constant for fast phase, c is the amplitude for slow phase, *d* is the rate constant for slow phase, t is time in seconds and y_0 accounts for the non-zero baseline.

3.2.8.2 Substrate Kinetic Isotope Effect

The experiments were performed under similar conditions as described in 3.2.8.1, except the substrates used were the NADPH and NADPD synthesized in the laboratory of Dr. Pablo Sobrado, not commercial products.

3.3 Results

3.3.1 Solvent Kinetic Isotope Effect

3.3.1.1 Steady State Kinetics of *wt*Fno in H_2O

For FO, the kinetic parameters K_m and $k_{cat,}$ were determined by fitting the plot (Figure 3.2a) of rate constant, *k (*sec^{-1}*)* versus varying FO concentration (μM) to the Michaelis-Menten hyperbolic equation (Equation 2).

The K_m and k_{cat} were 4.0 ± 0.4 μM and 5.3 ± 0.1 sec^{-1}, respectively. The kinetic parameters for NADPH were determined under the same conditions as described for FO. However, the plot of *k* (sec^{-1}) vs NADPH concentration did not display the typical hyperbola at NADPH concentrations greater than 100 μM (Figure 3.2b). The plot displayed non Michaelis-Menten behavior with increasing concentrations of NADPH, and had two phases. Each phase was fitted in a Lineweaver-Burk plot, and the steady state parameters for each phase were determined by using a double reciprocal plot. The macroscopic rate constants for the first and second phases are 4.16 ± 0.07 sec^{-1} and 5.41 ± 0.04 sec^{-1}, respectively. The values of K_m for the two phases were 2.3 ± 0.2 μM and 61 ± 6 μM, respectively (performed by Cuong Le) (44).

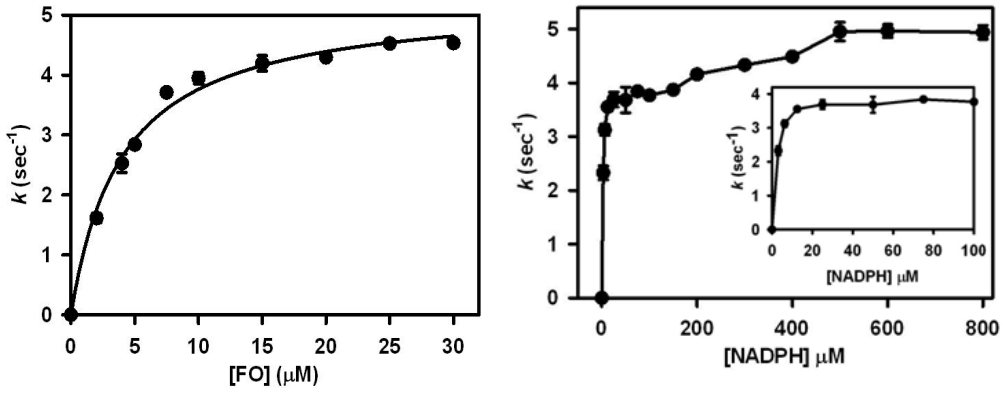

(a) (b)

Figure 3.2 Steady-state kinetics of reduction of FO by Fno for varying (a) [FO] in H_2O, (b) [NADPH] in H_2O (44)

3.3.1.2 Steady State Kinetics of *wt*Fno in D_2O

The steady state kinetic parameters for both FO and NADPH were determined under the same conditions as described in 3.3.1.1, the steady state kinetics of *wt*Fno in H_2O.

The kinetic parameters K_m and k_{cat} of FO in D_2O were 2.2 ± 0.1μM and 2.9 ± 0.6 sec^{-1}, respectively (Figure 3.3).

The plot of k (sec^{-1}) vs [NADPH] did not display the typical hyperbola at higher NADPH concentrations neither (Figure 3.4a). The steady state kinetic parameters for each phase were determined using Lineweaver-Burk plot as well (Figure 3.4b). The macroscopic rate constants for the first and second phases are 1.1 ± 0.1 sec^{-1} and 2.8 ± 0.4 sec^{-1}, respectively. The values of K_m were 20. ± 2 μM for the first phase and 980 ± 80 μM for the second phase.

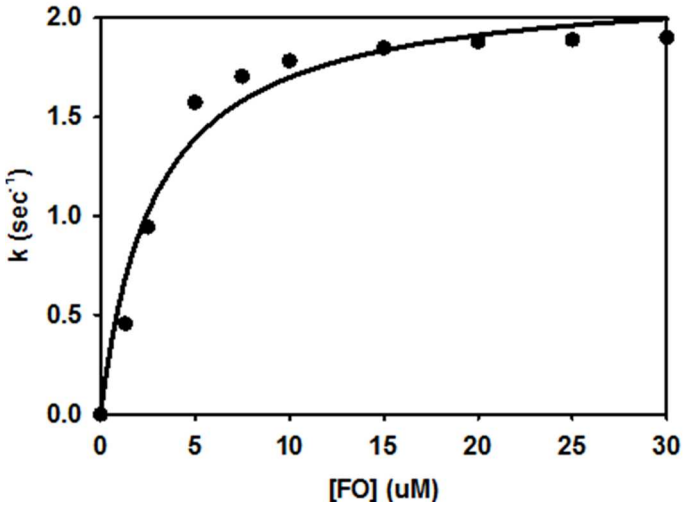

Figure 3.3 Steady-state kinetics of reduction of FO by Fno for varying [FO] in D_2O

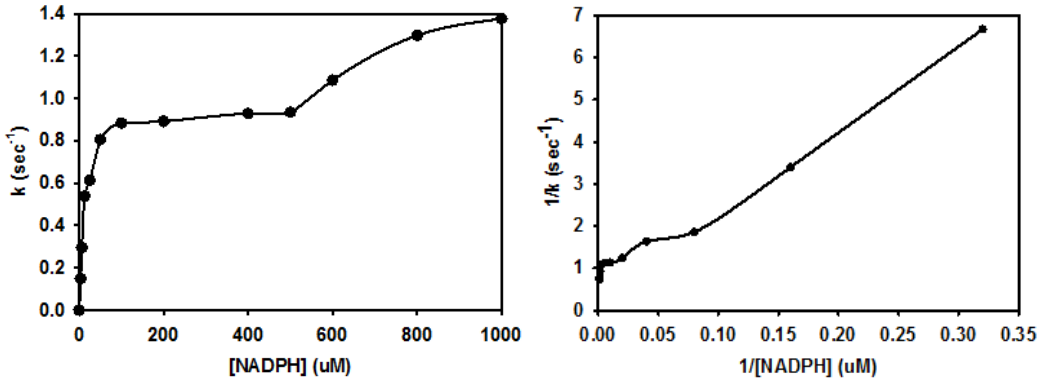

(a) (b)

Figure 3.4 Steady-state kinetics of reduction of FO by Fno with varying [NADPH] in D_2O (a) with double-reciprocal plot, (b) with not typical hyperbolic curve

3.3.1.3 Single Turnover Kinetics of *wt*Fno in H_2O and D_2O

A solution containing *wt*Fno was mixed with equal volumes of solutions containing FO and NADPH in the stopped-flow spectrophotometer. The reduction of the FO peak was monitored by absorbance changes at 420 nm.

Under single-turnover conditions, *k* values were determined by equation 4 and yielded 50 ± 4 s^{-1} for past phase and 6.04 ± 0.07 s^{-1} for H_2O solvent. For D_2O solvent, the rate constants were 50 ± 4 s^{-1} and 4.48 ± 0.09 s^{-1} for fast phase and slow phase respectively.

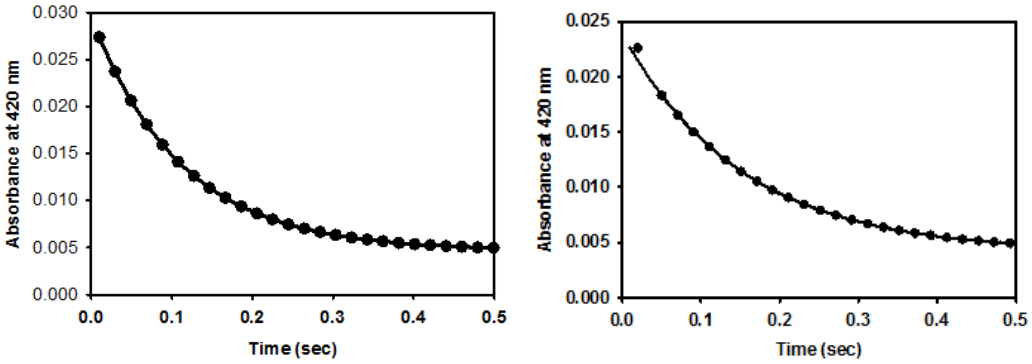

(a) (b)

Figure 3.5 Single turnover kinetics (a) in H_2O, (b) in D_2O

Table 3.1 Solvent KIE: steady-state kinetics of reduction of FO by Fno with varying [NADPH].

Solvent	**First phase *k* (s^{-1})**	**Second phase *k* (s^{-1})**
H_2O	4.16 ± 0.07	5.41 ± 0.04
D_2O	1.1 ± 0.1	2.8 ± 0.4

KIE	**3.8 ± 0.3**	**1.9 ± 0.3**

Table 3.2 Solvent KIE: steady-state kinetics of reduction of FO by Fno with varying [FO].

Solvent	***k*** **(s^{-1})**
H_2O	5.2 ± 0.1
D_2O	2.2 ± 0.1
KIE	**2.4 ± 0.1**

Table 3.3 Solvent KIE: single turnover kinetics of FO reduction by Fno.

Solvent	**Fast phase *k* (s^{-1})**	**Slow phase *k* (s^{-1})**
H_2O	50. ± 4	6.04 ± 0.07
D_2O	50. ± 4	4.48 ± 0.09
KIE	**1.00 ± 0.08**	**1.3 ± 0.1**

3.3.2 Substrate KIE

3.3.2.1 Steady State Kinetics for NADPH and NADPD

Again, the plot of *k* (sec^{-1}) vs [NADPH] did not display the typical hyperbola at higher NADPH concentrations (Figure 3.6a). The steady state kinetic parameters for each phase were determined using a Lineweaver-Burk plot. The macroscopic rate constants for the first and second phases are 1.32 ± 0.02 sec^{-1} and 3.3 ± 0.2 sec^{-1}, respectively. The values of K_m were 3.9 ± 0.1 μM for the first phase and 460 ± 40 μM for the second phase.

The plot of k (sec^{-1}) vs [NADPD] did not display the typical hyperbola at higher NADPD concentrations either (Figure 3.6b). The steady state kinetic parameters for each phase were determined using a Lineweaver-Burk plot as well. The macroscopic rate constants for the first and second phases are 0.82 ± 0.03 sec^{-1} and 2.6 ± 0.2 sec^{-1}, respectively. The values of K_m were 3.7 ± 0.3 μM for the first phase and 610 ± 60 μM for the second phase.

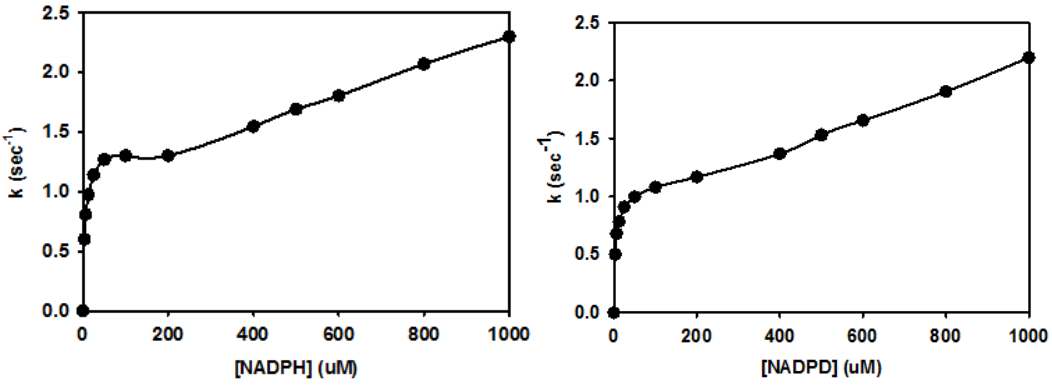

(a) (b)

Figure 3.6 Steady-state kinetics of reduction of FO by Fno with (a) varying [NADPH], (b) varying [NADPD].

3.3.2.2 Single Turnover Kinetics for NADPH and NADPD

Under single-turnover conditions, for synthesized NADPH, k was determined to be 31 ± 2 s^{-1} and 4.7 ± 0.2 s^{-1} for fast phase and slow phase respectively. For NADPD, k was 28 ± 3 s^{-1} for fast phase and 4.13 ± 0.09 s^{-1} for slow phase.

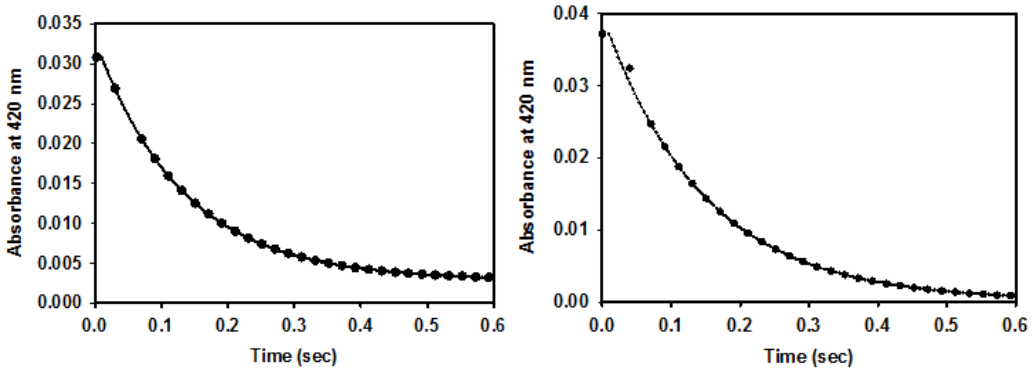

(a) (b)

Figure 3.7 Single turnover kinetics of (a) NADPH, (b) NADPD

Table 3.4 Substrate KIE: steady-state kinetics of reduction of FO by Fno .

Substrate	First phase k (sec-1)	Second phase k (sec-1)
NADPH	1.32 ± 0.02	3.3 ± 0.2
NADPD	0.82 ± 0.03	2.65 ± 0.02
KIE	**1.61 ± 0.06**	**1.3 ± 0.1**

Table 3.5 Substrate KIE: single turnover kinetics of FO reduction by Fno

Substrate	Fast phase *k* (s^{-1})	Slow phase *k* (s^{-1})
NADPH	31 ± 2	4.7 ± 0.2
NADPD	28 ± 3	4.13 ± 0.09
KIE	**1.11 ± 0.08**	**1.1 ± 0.1**

3.3.2.3 Discussion

Based upon steady state and single turnover kinetics of substrates NADPH and NADPD, the KIE in steady state were 1.61 ± 0.06 and 1.3 ± 0.1, and in single turnover kinetics were 1.11 ± 0.08 and 1.1 ± 0.1 as shown in Table 3.4 and 3.5. The KIE values reflected a secondary kinetic isotope effect as we expected, since the synthesized NADPD was *pro*-R labeled and hydride transfer only occurs at *pro*-S position. Sp^3 carbon that the deuterium bound to was converted to sp^2 carbon, we should be able to see a normal secondary KIE effect. However, *Pro*-S labeled NADPD studying is necessary to get a better understanding for Fno reaction mechanism.

For the solvent effects, we found that in steady state, KIE values for both NADPH and FO reflected a primary kinetic isotope effect (shown in Table 3.1, 3.2), in the single turnover experiments, however, a secondary kinetic isotope effect was observed (Table 3.3). Interpretation of these data yields the conclusion that the solvent participated in the reaction's rate-limiting step. In solvent KIE experiments the solvent can commonly participate in three ways (53, 54). First, the solvent can assist in the stabilization of an intermediate. However, this is not likely to produce a large isotope effect, as seen in the steady-state experiments. Next, the exchange of hydrogen for deuterium. If the *pro*-S position H could be exchanged to D, this could explain the large KIE as we seen in steady state kinetics. However, the exchange of hydrogen for deuterium normally refers to proton transfer, not hydride transfer.

The final mechanism for seeing solvent KIE could be if the deuterium participates in the reaction as a proton donor in the rate-limiting step. The *pro*-S hydride is transfered from NADPH to F_{420} cofactor. The electrons then flow through the sp^2 hybridized carbons down to nitrogen, giving nitrogen a formal negative charge. Once F_{420} cofactor has lost conjunction in this area of the molecule, it loses the absorbance at 420 nm. This was the

observation made in the single turnover kinetic studies. However, a nitrogen atom possessing a negative charge is not stable. To alleviate the charge, the nitrogen will extract a deuterium the solvent D_2O, which breaks the O-D bond and forms a new bond between nitrogen and deuterium, which is the rate-limiting step as was seen in the steady state kinetics experiments.

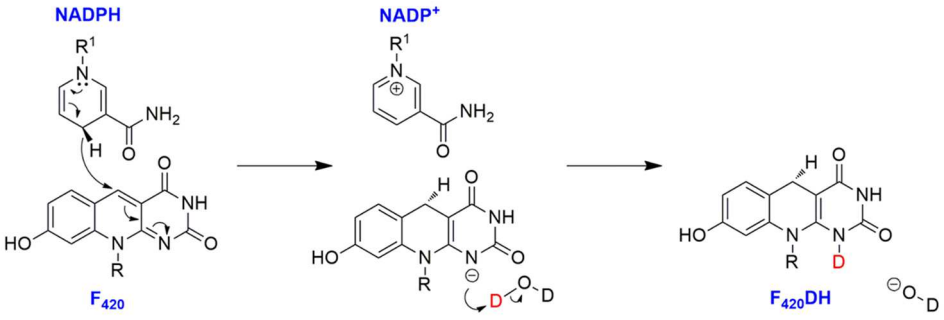

3.3.2.4 Summary

Hydride transfer is of great importance to many biological processes. The measurement of kinetic isotope effect can play a significant role in clarifying the mechanistic and kinetic details of complex enzymatic hydride transfer reactions (47).

In future work, *pro*-S labeled NADPH, temperature-dependent KIE and Fno variants KIE experiments are necessary to get more detailed information about the regulatory kinetic mechanism of Fno.

References

1. DiMarco, A.; Bobik, T.; Wolfe, R. Unusual Coenzymes of Methanogenesis. *Annu. Rev. Biochem*. **1990**, *59*, 355-394.

2. Cheeseman, P.; Toms-Wood, A.; Wolfe, R. Isolation and Properties of a Fluorescent Compound, Factor 420, from *Methanobacterium* Strain M.o.H. J. *Bacteriol.* ***1972****, 112,* 527–531.

3. Eirich, L.; Vogels, G.; Wolfe, R. Distribution of Coenzyme F_{420} from *Meththanobacterium. Biochemistry* **1979**, *17*, 4583-4593.

4. Bashiri, G.; et al. Crystal Structures of F_{420}-dependent Glucose-6-Phosphate Dehydrogenase FGD1 Involved in the Activation of the Anti-tuberculosis Drug Candidate PA-824 Reveal the Basis of Coenzyme and Substrate Binding. *J.Bio.Chem*. **2008**, *283,* 17531-17541.

5. Graupner, M.; White, R. *Methanococcusjannaschii* Coenzyme F_{420} Analogs Contain a Terminal α-Linked Glutamate. *J. Bacteriol.* **2003,** *185*, 662-4665.

6. Purwantini, E., Coenzyme F_{420}: Factors Affecting Its Purification from *Methanobacterium Thermoautotrophicum* and Its Conversion to F_{390} and Effect of Temperature on the Spectral Properties of Coenzyme F_{420} and Related Compounds. University of Iowa: **1991**.

7. Bashiri, G.; et al. Metebolic Engineering of Cofactor F_{420} Production in *Mycobacterium Smegmatis. Plos One*, **2010**, *5*, 15803.

8. Kunow, J.; Schworer, B.; Stetter, K.; Thauer, R. A F_{420}-dependent $NADP^+$ Reductase in the Extremely Thermophilic Sulfate Reducing *Archaeoglobus fulgidus. Arch. Microbiol*. **1993,** *160,* 199-205.

9. Warkentin, E.; et al. Structure of $F_{420}H_2$:$NADP^+$ Oxidoreductase With and Without its Substrate Bound. *EMBO J.* **2001,** *20*, 6561-6569.

10. Isabelle, D.; et al. Large-Scale Production of Coenzyme F_{420}-5,6 by Using *Mycobacterium Smegmatis*. *Appl. Environ. Microbiol*. **2002,** *68*, 5750-5755.

11. Klein, A.; Berk, H.; Purwantini, E.; Daniels, L.; Thauer, R. Si-face Stereospecificity at C5 of Coenzyme F_{420} for F_{420}-dependent Glucose-6-Phosphate Dehydrogenase from *Mecobateriumsmegmatis and* F_{420}-Dependent Alcohol Dehydrogenase from *Methanoculleusthermophicius. Eur. J. Biochem*, **1996**. *239*, 93-97.

12. Jacobson, F.; Daniels, L.; Fox, J.; Walsh, C. Orme-Johnson, W. Purification and Properties of an 8-Hydroxy-5-deazaflavin-Reducing Hydrogenase from Methanobacterium Thermoautotrophicum. *J. Biol. Chem.* **1982**, *257*, 3385–3388.

13. Deppenmeier, U.; Blaut, M.; Mahlmann, A.; Gottschalk, G. Membranebound $F_{420}H_2$-Dependent Heterodisulfide Reductase in Methanogenic Bacteriumstrain Gol and *Methanolobus Tindarius*. *FEBS Lett.* **1990**, *261*,199–203.

14. Seedorf, H.; Dreisbach, A.; Hedderich, R.; Shima, S.; Thauer, R. $F_{420}H_2$ Oxidase (FprA) from *Methanobrevibacter Arboriphilus*, a Coenzyme F_{420}-Dependent Enzyme Involved in O_2 Detoxification. *Arch Microbiol*. **2004**, *182*, 126–137.

15. Tzeng, S.; Wolfe, R.; Bryant, M. Factor 420-Dependent Pyridine Nucleotide-Linked Hydrogenase System of *Methanobacterium Ruminantium*. *J. Bacteriol.* **1975**, *121*, 184–191.

16. Deppenmeier, U,; Blaut, M.; Mahlmann, A.; Gottschalk, G. Reduced Coenzyme F_{420}: Heterodisulfide Oxidoreductase, a Proton-Translocating Redox System in Methanogenic Bacteria*. Proc. Natl. Acad. Sci. USA.* **1990**, *87*, 9449–9453.

17. Kunow, J.; Linder, D.; Stetter; K.; Thauer, R. $F_{420}H_2$: Quinone Oxidoreductase from *Archaeoglobus Fulgidus*. Characterization of a Membranebound Multisubunit Complex Containing FAD and Iron-Sulfur Clusters. Eur. *J. Biochem*. **1994**, *223*, 503–511.

18. Tzeng, SF.; Bryant, M.; Wolfe, R. Factor 420-Dependent Pyridine Nucleotide-Linked Formate Metabolism of *Methanobacterium Ruminantium*. *J. Bacteriol*. **1975**, *121*, 192–196.

19. Zeikus, J.; Fuchs, G.; Kenealy, W.; Thauer, R. Oxidoreductases Involved in Cell Carbon Synthesis of Methanobacterium Thermoautotrophicum. *J. Bacteriol*. **1977**, *132*, 604–613.

20. Hartzell, P.; Zvilius, G.; Escalante-Semerena, J.; Donnelly, M. Coenzyme F_{420} Dependence of the Methylenetetrahydromethanopterin Dehydrogenase of *Methanobacterium Thermoautotrophicum*. *Biochem. Biophys. Res. Commum*. **1985**, *133*, 884–890.

21. Ma, K.; Thauer, R. Purification and Properties of N5, N10-Methylenetetrahydromethanopterin Reductase from *Methanobacterium Thermoautotrophicum* (strain Marburg). *Eur. J. Biochem*. **1990**, *191*, 187–193.

22. Widdel, F.; Wolfe, R. Expression of Secondary Alcohol Dehydrogenase in Methanogenic Bacteria and Purification of the F_{420}-Specific Enzyme from *Methanogenium Thermophilum* Strain TCI. *Arch Microbiol*. **1989**, *152*, 322–328.

23. Purwantini, E.; Daniels, L. Purification of a Novel Coenzyme F_{420}-Dependent Glucose-6-Phosphate Dehydrogenase from Mycobacterium Smegmatis. *J. Bacteriol*. **1996**, *178*, 2861–2866.

24. Taylor, M.; et al. Identification and Characterization of Two Families of $F_{420}H_2$-Dependent Reductases from Mycobacteria that Catalyze Aflatoxin Degradation. *Mol Microbiol*. **2010**, *78*, 561–575.

25. Singh, R.; et al. PA-824 Kills Nonreplicating *Mycobacterium* Tuberculosis by Intracellular NO Release. *Science*, **2008**, *322*, 1392-1395.

26. Eker, A.; Hessels, J.; Velde, J. Photoreactivating Enzyme from the Green Alga *Scenedesmus Acutus*. Evidence for the Presence of Two Different Flavin Chromophores. *Biochemistry* **1988**, *27*, 1758–1765.

27. Eker, A.; Kooiman, P.; Hessels, J.; Yasui, A. DNA Photoreactivating Enzyme from the Cyanobacterium *Anacystis Nidulans. J. Biol. Chem*. **1990**, *265*, 8009–8015.

28. Glas, A.; Maul, M.; Cryle, M.; Barends, T.; Schneider, S.; et al. The Archaeal Cofactor F0 is a Light-Harvesting Antenna Chromophore in Eukaryotes. *Proc. Natl. Acad. Sci. USA*. **2009**, *106*, 11540–11545.

29. Kiener, A.; Gall, R.; Rechsteiner, T.; Leisinger, T. Photoreactivation in *Methanobacterium thermoautotrophicum*. *Arch Microbiol*. **1985**, *143*, 147–150.

30. Hossain, M.; Le, C.; Joseph, E.; Nguyen, T.; Johnson-Winters, K.; Foss, F. W., Jr. Convenient Synthesis of Deazaflavin Cofactor FO and its Activity in F_{420}-Dependent $NADP^+$ Reductase. *Org. Biomol. Chem.* **2015**, *13*, 5082–5085.

31. Ashton, W.; Brown, R.; Jacobsen, F.; Walsh, C. *J. Am. Chem. Soc*. **1979**, *101*, 4419–4420.

32. Tanaka, k.; Kimachi, T.; Kawase, M.; Yoneda, F. *J. Chem. Soc. Chem. Commun.* **1988**, 524–526.

33. Corbett, E.L., et al. The Growing Burden of Tuberculosis: Global Trends and Interactions with the HIV Epidemic*. Arch. Intern. Med* **2003**, *163*, 1009-1021.

34. Global Tuberculosis Control. 2010. World Health Organization.

35. Young, D.; Perkins, M.; Duncan, K.; Barry, C. Confronting the Scientific Obstacles to Global Control of Tuberculosis*. J. Clin. Invest*. **2008**, *118*, 1255-1265.

36. Post, F.; et al. Multi-Drug-Resistant Tuberculosis in HIV Positive Patients in Eastern Europe*, J. Infect*. **2013**. *1*, 1-5.

37. Manjunatha, U.; et al. Identification of a Nitroimidazo-Oxazine-Specific Protein Involved in PA-824 Resistance in *Mycobacterium Tuberculosis. PNAS*. **2006**, *10*, 431-436.

38.Bashiri, G.; Squire, C.; Baker, E.; Moreland, N. Expression, Purification and Crystallization of Native and Selenomethionine Labeled *Mycobacterium Tuberculosis* FGD1 (Rv0407) using a *Mycobecteriumsmegmatis* Expression System. *Protein Expression and Purif* **2007,** *54*, 38-44.

39. Goldstone, R.; Moreland, N.; Bashiri, G.; Baker, E.; Lott, J. A New Gateway Vector and Expression in *Mycobacterimsmegmatis. Protein Expression and Purif.* **2008**, *57*, 81-87.

40. Yamazaki, S.;Tsai, L. Stereochemical Studies of 8-hydroxy-5-deazaflavin-dependent NADP+ reductase from *Methanococcus vannielii. J. Biol. Chem.* **1980**, *255*, 9025–9027.

41. Berk, H.; THauer, R. $F_{420}H_2$: $NADP^+$ Oxidoreductase from *Methanobacterium Thermoautotrophicum*: Identification of the Encoding Gene Via Functional Overexpression in Escherichia Coli. *FEBS Lett*. **1998**, *483*, 124-126.

42. Jacobson, F.; Walsh, C. Properties of 7,8-Didemethyl-8-hydroxy-5-Deazaflavins Relevant to Redox Coenzyme Function in Methanogen Metabolism. *Biochemistry* **1984**, *23*, 979–988.

43. Eker, A.; et al. Characterization of an 8-Hydroxy-5-deazaflavin: NADPH Oxidoreductase from Streptomyces *Griseus. Biochim. Biophys. Acta*. **1989**, *990*, 80-86.

44. Joseph, E.; Le, C.Q.; Nguyen, T.; Hossain, M.S.; Oyugi, M.; Johnson-Winters, K.; and Foss, F. W., Jr. Evidence of Negative Cooperativity and Half-Site Reactivity within an F_{420}-Dependent Enzyme: Kinetic Analysis of $F_{420}H_2$:$NADP^+$ Oxidoreductase. Biochemistry, submitted for publication.

45 Koshland, D. Jr., Nemethy, G.; and Filmer, D. Comparison of Experimental Binding Data and Theoretical Models in Proteins Containing Subunits, *Biochemistry* **1996**, *5*, 365–385.

46 Kohen , A.; Klinman, J. Hydrogen-Tunneling in *Biology. Chem. Biol.* **1999**, *6,* 191-198.

47. Allemann, R.; Scrutton, N. Quantum Tunnelling in Enzyme-Catalyzed Reactions; RSC Publishing: Cambridge, UK, **2009**; 1st ed.

48. Stojkovic, V.; Preissinotti, L.;Lee. J.; Benkovic, S., Kohen, A. The Effect of Active-site Isoleucine to Alanine Mutation on the DHFR Catalyzed Hydride-transfer. *J. Am. Chem. Soc.* **2010,** *46,* 8974-8976.

49. Wang, L.; Goodey, N.M.; Benkovic, S.J.; and Kohen,A. Proc. Natl. Acad. Sci. U. S. A., **2006**, 103, 15753–15758.

50. Truhlar, D. G.; in Isotope effects in chemistry and biology, ed. Kohen, A. and Limbach, H.H.;CRC Press, Boca Raton, FL, **2006**, 579–620.

51. Stojkovic, V.; Preissinotti, L.; Willmer, D.; Benkovic, S., Kohen, A. Effects of the Donor-Acceptor Distance and Dynamics on Hydride Tunneling in the Dihydrofolate Reducase Catalyzed Reaction. *J. Am. Chem. Soc.* **2012,** *134,* 1738-1745.

52. Berk, H.; Thauer, R. $F_{420}H_2$: $NADP^+$ Oxidoreductase From *Methanobacteriumthermoautotrophicum*: Identification of the Encoding Gene Via Functional Overexpression in *Escherichia coli. FEBS Lett*. **1998,** *438*, 124-126.

53. March, J., Smith, M.B.; March's Advanced Organic Chemistry; John Wiley & Sons, Inc.: Hoboken, NJ, **2007**; 6th ed.

54. Chang, R.; Physical Chemistry for the Chemical and Biological Sciences; University Science Books: Sausalito, CA, **2000**, 480-483.

Biographical Information

Siqi Du was born in Changchun, China. She received her Bachelor's Degree in Bioengineering from Huaihai Institute of Technology in 2013.

In August of 2013 she began her graduate studies towards a Master of Science in Chemistry at the University of Texas Arlington under the supervision of Dr. Johnson-Winters. The research work is focused on enzyme purification and enzyme kinetics.

Siqi Du received her Master of Science in August 2015. She plans to continue to pursue a PhD in Chemistry.